Hydromagnetic Nanofluids flow through porous media with thermal radiation, chemical reaction and viscous dissipation using spectral relaxation method

Nageeb A.H Haroun[1], S. Mondal[1,a)] and P. Sibanda[1]

[1]School of Mathematics, Statistics and Computer Science, University of KwaZulu-Natal
Private Bag X01 Scottsville 3209, Pietermaritzburg, South Africa

[a)]Corresponding author and Presenting author: sabya.mondal.2007@gmail.com

Abstract.

We investigate the convective heat and mass transfer in magnetohydrodynamic a nanofluid through a porous medium over a stretching sheet subject to a magnetic field, heat generation, thermal radiation, viscous dissipation and chemical reaction effects. The effects of porosity, heat generation, thermal radiation, magnetic field, viscous dissipation and chemical reaction to the flow field are thoroughly explained for various values of the governing parameters. We have further assumed that the nanoparticle volume fraction at the wall may be actively controlled. Two types of nanofluids, namely Cu-water and Al_2O_3-water are studied. The physical problem is modeled using systems of nonlinear differential equations which have been solved numerically using the spectral relaxation method. Comparing the results with those previously published results in the literature shows excellent agreement.

Keywords: MHD Nanofluids flow; Porous media; Thermal radiation; Spectral relaxation method.

Introduction

Nanofluids are suspensions of metallic, non-metallic or polymeric nano-sized powders in a base liquid which are employed to increase the heat transfer rate in various applications. In recent years, the concept of nanofluid has been proposed as a route for increasing the performance of heat transfer liquids. Due to the increasing importance of nanofluids, there is an enormous amount of literature on convective transport of nanofluids and problems linked to a stretching surface. Today nanofluid are sought to have more range of applications in power generation in nuclear reactors, medical application, biomedical industry, detergency, and more specifically in any heat removal involved industrial applications. The ongoing work ever since then has extended to utilization of nanofluids in microelectronics, fuel cells, pharmaceutical processes, vehicle thermal management, domestic refrigerator, chillers, heat exchanger, nuclear reactor coolant, grinding, machining, space technology, defence and ships, and boiler flue gas temperature reduction. The majority of the previous studies have been restricted to boundary layer flow and heat transfer in nanofluids. Following the early work by Crane [1], Khan and Pop [2] were the first to work on nanofluid flow due to stretching sheet. A mathematical analysis of momentum and heat transfer characteristics of the boundary layer flow of an incompressible and electrically conducting viscoelastic fluid over a linear stretching sheet was carried out by Abd El-Aziz [3]. In addition, radiation effects on the viscous flow of a nanofluid and heat transfer over a nonlinearly stretching sheet were studied by Hady et al. [4]. Theoretical studies include, for example, modelling unsteady boundary layer flow of a nanofluid over a permeable stretching/shrinking sheet by Bachok et al. [5]. Rohni et al. [6] developed a numerical solution for the unsteady flow over a continuously shrinking surface with wall mass suction using the nanofluid model proposed by Buongiorno [7]. The effect of an applied magnetic field on nanofluids has substantial applications in chemistry, physics and engineering. These include cooling of continuous filaments, in the process of drawing, annealing and thinning of copper wire. Drawing such strips through an electrically conducting fluid subject to a magnetic field can control the rate of cooling and stretching, thereby furthering the desired characteristics of the final product. In other work, Jafar et al. [8] studied the effects of magnetohydrodynamic(MHD) flow and heat transfer due to a stretching/shrinking sheet with an external magnetic field, viscous dissipation and joule effects. Murthy and Singh [9] studied viscous dissipation on non-Darcy natural convection regime in porous media saturated with Newtonian fluid. In the past few years, convective heat and mass transfer in nanofluids has become a topic of major contemporary interest. In this paper we examine the study analyzed of magneto-hydrodynamics (MHD), heat and mass transfer in nanofluid flow over a stretching sheet subject to Porous media, hydromagnetic, heat generation, thermal radiation, viscous dissipation, chemical re- action and Soret effects. The spectral relaxation method (SRM) was proposed by Motsa [10]. It is used to solve the governing partial differential equations numerically. This spectral relaxation method has been successfully applied to other problems of fluid mechanics and heat transfer. In this paper we discuss the fluid flow and heat transfer as well as highlight the strengths of the solution method.

Governing Equations

Consider the two-dimensional steady boundary layer flow of an incompressible heat and mass transfer nanofluid past a stretching sheet. The origin of the system is located at the slit from which the sheet is drawn. In this coordinate frame the x-axis is taken along the direction of the continuous stretching surface. The y-axis is measured normal to the surface of the sheet. It is assumed that the induced magnetic field is negligible in comparison to the applied magnetic field. It is assumed that the induced magnetic field, the external electric field and the electric field due to the polarization of charges are negligible in comparison to the applied magnetic field. In addition to these, the effects of chemical heating, agglomeration and sedimentation of nanoparticles are not included in the work.
The fluid is a water based nanofluid containing two different types of nanoparticles; Copper (Cu) and Alumina (Al_2O_3) nanoparticles. It is assumed that the base fluid and the nanoparticles are in thermal equilibrium and no slip occurs between them. The thermophysical properties of the nanofluid are given in Table 1.
With the above assumptions, the governing boundary layer equations of the nanofluid flow, the continuity, momentum, energy and the concentration fields with diffusion with radiation, heat generation, viscous dissipation and chemical reaction effects can be written in dimensional form as proposed by Tiwari and Das [11]

$$\frac{\partial u}{\partial x}+\frac{\partial v}{\partial y} = 0, \tag{1}$$

$$u\frac{\partial u}{\partial x}+v\frac{\partial u}{\partial y}=\frac{\mu_{nf}}{\rho_{nf}}\frac{\partial^2 u}{\partial y^2}-\left\{\frac{\mu_{nf}}{\rho_{nf}}\frac{1}{K}+\frac{\sigma B_0^2}{\rho_{nf}}\right\}u, \tag{2}$$

$$u\frac{\partial T}{\partial x}+v\frac{\partial T}{\partial y}=\alpha_{nf}\frac{\partial^2 T}{\partial y^2}+\frac{Q}{(\rho c_p)_{nf}}(T-T_\infty)+\frac{1}{(\rho c_p)_{nf}}\frac{16\sigma^* T_\infty^3}{3K^*}\frac{\partial^2 T}{\partial^2 y}+\frac{\mu_{nf}}{((\rho c_p)_{nf}}\left(\frac{\partial u}{\partial y}\right)^2, \tag{3}$$

$$u\frac{\partial C}{\partial x}+v\frac{\partial C}{\partial y}=D_B\frac{\partial^2 C}{\partial y^2}+\frac{D_T}{T_\infty}\frac{\partial^2 T}{\partial y^2}-K_0(C-C_\infty), \tag{4}$$

Here q_r is the radiation heat flux given by

$$q_r=-\frac{4\sigma^*}{3K^*}\frac{\partial T^4}{\partial y} \tag{5}$$

where σ^* is the Stefen-Boltzmann constant and K^* is the Rosseland mean absorption coefficient. The temperature variation T^4 is expanded in a Taylor series expansion form. Neglecting higher order terms and expanding T^4 about T_∞ we obtain,$T^4 \cong 4T_\infty^3 T-3T_\infty^4$. where u and v are the fluid velocity and normal velocity components along $x-$ and $y-$directions, respectively, $\mu_{nf}, \rho_{nf}, \alpha_{nf}$ are the effective dynamic viscosity of the nanofluid, nanofluid density and the thermal diffusivity of the nanofluid respectively. The boundary conditions for equations (1) - (4) are as follows

$$\begin{aligned} &u=ax,\ v=0,\ T=T_{\mathrm{w}}(x)=T_\infty+H\left(\tfrac{x}{\omega}\right)^2,\\ &C=C_{\mathrm{w}}(x)=C_\infty+Q\left(\tfrac{x}{\omega}\right)^2 \quad \text{at} \quad y=0,\\ &u\to 0,\ T\to T_\infty,\ C\to C_\infty \quad \text{as} \quad y\to\infty, \end{aligned} \tag{6}$$

where Q, H and a are constants, $a>0$ and ω is the characteristic length. The effective dynamic viscosity of the nanofluid was given by Brinkman [14] as

$$\mu_{nf}=\frac{\mu_f}{(1-\phi)^{2.5}}, \tag{7}$$

where ϕ and μ_f are the solid volume fraction of nanoparticles and the dynamic viscosity of the base fluid. In equations (1) to (4) the heat capacitance of the nanofluid and the thermal conductivity of nanofluids restricted to spherical nanoparticles is approximated by the Maxwell-Garnett model (see Maxwell Garnett [15]).

$$\begin{aligned} &(\rho c_p)_{nf}=(1-\phi)(\rho c_p)_f+\phi(\rho c_p)_s,\\ &\rho_{nf}=(1-\phi)\rho_f+\phi\rho_s, \nu_{nf}=\tfrac{\mu_{nf}}{\rho_{nf}},\\ &\alpha_{nf}=\tfrac{k_{nf}}{(\rho c_p)_{nf}}, k_{nf}=k_f\left[\tfrac{(k_s+k_f)-2\phi(k_f-k_s)}{(k_s+k_f)+\phi(k_f-k_s)}\right], \end{aligned} \tag{8}$$

where ν_{nf}, ρ_{nf}, $(\rho c_p)_{nf}$, k_{nf}, k_f, k_s, ρ_s, $(\rho c_p)_f$, $(\rho c_p)_s$ are the nanofluid kinematic viscosity, the electrical conductivity, the nanofluid heat capacitance, thermal conductivity of the nanofluid, thermal conductivity of the fluid, the thermal conductivity of the solid fractions, the density of the solid fractions, the heat capacity of base fluid, the effective heat capacity of nanoparticles, respectively, (see Abu-Nada [16] and Kameswaran et al. [18]).
The continuity equation (1) is satisfied by introducing a stream function $\psi(x, y)$ such that

$$u = \frac{\partial \psi}{\partial y}, v = -\frac{\partial \psi}{\partial x}. \tag{9}$$

Introducing the following non-dimensional variables,

$$\psi = \left[a\nu_f\right]^{\frac{1}{2}} \; xf(\eta), u = axf'(\eta), v = -\left(a\nu_f\right) f(\eta), \tag{10}$$

$$\theta(\eta) = \frac{T - T_\infty}{T_\mathrm{w} - T_\infty}, \varphi(\eta) = \frac{C - C_\infty}{C_\mathrm{w} - C_\infty}, \eta = \left[\frac{a}{\nu_f}\right]^{\frac{1}{2}} \; y \tag{11}$$

where η, is the similarity variable, $f(\eta)$ is the dimensionless stream function, $\theta(\eta)$ is the dimensionless temperature and $\varphi(\eta)$ is the dimensionless concentration. By using (7), (8) and (11) the governing equations (2), (4) and (3) along with the boundary conditions (6) are reduced to the following two-point boundary value problem:

$$f''' + \phi_1 \left[ff'' - f'^2 - \frac{1}{\phi_2} Mf'\right] - K_1 f' = 0, \tag{12}$$

$$\left(1 + \frac{4R}{3}\right)\theta'' + Pr\frac{k_f}{k_{nf}}\phi_3 \left[f\theta' - 2f'\theta + \delta\theta + \frac{E_c}{\phi_4} f''^2\right] = 0, \tag{13}$$

$$\varphi'' + Sc\,(f\varphi' - 2f'\varphi + \gamma\varphi) + Sr\theta'' = 0, \tag{14}$$

subject to the boundary conditions

$$f(0) = 0, f'(0) = 1, \theta(0) = 1, \varphi(0) = 1, \eta = 0, \tag{15}$$

$$f'(\infty) \to 0, \theta(\infty) \to 0, \varphi(\infty) \to 0, \eta \to \infty, \tag{16}$$

Where primes denote differentiation with respect to η, $\alpha_f = k_f/(\rho c_p)_f$ and $\nu_f = \mu_f/\rho_f$ are the thermal diffusivity and kinetic viscosity of the base fluid, respectively. Other non-dimensional parameters appearing in equations (12) to (14) are M, K_1, R, Pr, δ, E_c, Sc, γ and Sr denote the magnetic parameter, porous medium parameter, thermal radiation parameter, Prandtl number, heat generation parameter, Eckert number, Schmidt number, scaled chemical reaction parameter and Soret number. These parameters are defined mathematically as

$$M = \frac{\sigma B_0^2}{a\rho_f}, K_1 = \frac{\nu_f}{ak}, R = \frac{4\sigma^* T_\infty^3}{k^* k_{nf}}, Sc = \frac{\nu_f}{D}, \tag{17}$$

$$Pr = \frac{\nu_f (\rho c_p)_f}{k_f}, \delta = \frac{Q}{a(\rho c_p)_{nf}}, \gamma = \frac{K_0}{a}, \tag{18}$$

$$E_c = \frac{u_w^2}{(T_w - T_\infty)(c_p)_f}, Sr = \frac{D_1(T_w - T_\infty)}{D(C_w - C_\infty)}. \tag{19}$$

The nanoparticle volume fraction ϕ_1 and ϕ_2 are defined as

$$\begin{gathered}\phi_1 = (1-\phi)^{2.5}\left[1 - \phi + \phi\left(\frac{\rho_s}{\rho_f}\right)\right], \phi_2 = 1 - \phi + \phi\frac{(\rho_s)}{(\rho_f)}, \\ \phi_3 = 1 - \phi + \phi\frac{(\rho c_p)_s}{(\rho c_p)_f}, \phi_4 = (1-\phi)^{2.5}\left[1 - \phi + \phi\frac{(\rho c_p)_s}{(\rho c_p)_f}\right].\end{gathered} \tag{20}$$

Skin friction, heat and mass transfer coefficients

The quantities of engineering interest are the skin friction coefficient C_f, the local Nusselt number Nu_x and the local Sherwood number Sh_x characterize the surface drag, wall heat and mass transfer rates respectively. The shearing stress at the surface of the wall τ_w is defined as

$$\tau_w = -\mu_{nf}\left(\frac{\partial u}{\partial y}\right)_{y=0} = -\frac{1}{(1-\phi)^{2.5}}\rho_f \sqrt{\nu_f a^3}\; x\, f''(0), \tag{21}$$

where μ_{nf} is the coefficient of viscosity. The skin friction coefficient is obtained as

$$C_{fx} = \frac{2\tau_w}{\rho_f U_w^2}, \tag{22}$$

and using equation (21) in (22) we obtained

$$\frac{1}{2}(1-\phi)^{2.5} \ \ C_{fx} = -\,Re_x^{-\frac{1}{2}} f''(0). \tag{23}$$

The heat transfer rate at the surface flux at the wall is defined as

$$q_w = -k_{nf}\left(\frac{\partial T}{\partial y}\right)_{y=0} = -k_{nf}\frac{(T_w - T_\infty)}{x}\sqrt{\frac{U_w x}{\nu_f}}\theta'(0), \tag{24}$$

where k_{nf} is the thermal conductivity of the nanofluid. The local Nusselt number is defined as

$$Nu_x = \frac{x q_w}{k_f (T_w - T_\infty)}. \tag{25}$$

Using equation (24) in equation (25), the dimensionless wall heat transfer rate is obtained as

$$\left(\frac{k_f}{k_{nf}}\right) Nu_x = -\,Re_x^{\frac{1}{2}}\ \theta'(0). \tag{26}$$

The mass flux at the wall surface is defined as

$$q_m = -D\left(\frac{\partial C}{\partial y}\right)_{y=0} = -DQ\left(\frac{x}{\omega}\right)^2 \sqrt{\frac{a}{\nu_f}}\ \ \varphi'(0), \tag{27}$$

and the local Sherwood number is obtained as

$$Sh_x = \frac{x q_m}{D\,(C_w - C_\infty)}. \tag{28}$$

The dimensionless wall mass transfer rate is obtained as

$$Sh_x = -\,Re_x^{\frac{1}{2}}\ \varphi'(0), \tag{29}$$

where Re_x represents the local Reynolds number and is defined as

$$Re_x = \frac{x u_w}{\nu_f}. \tag{30}$$

Method of Solution

The equations (12) to (14) are highly non-linear, it is difficult to find the closed form solutions. Thus, the solutions of these equations with the boundary conditions 15 and 16 were solved numerically using the SRM, Motsa [10].
The SRM is an iterative procedure that employs the Gauss-Seidel type of relaxation approach to linearise and decouple the system of differential equations. The linear terms in each equation is evaluated at the current iteration level (denoted by $r+1$) and non-linear terms are assumed to be known from the previous iteration level (denoted by r). The linearised form of (12) to (14) is

$$f'''_{r+1} + a_{1,r} f''_{r+1} - a_{2,r} f'_{r+1} = R_{1,r}, \tag{31}$$

$$(1 + \tfrac{4R}{3})\theta''_{r+1} + b_{1,r}\theta'_{r+1} + b_{2,r}\theta_{r+1} = R_{2,r},, \tag{32}$$

$$\varphi''_{r+1} + c_{1,r}\varphi'_{r+1} + c_{2,r}\varphi_{r+1} = R_{3,r}, \tag{33}$$

Results and Discussion

The nonlinear boundary value problem 12 to 14 subject to the boundary conditions 15 and 16 connot be solved in closed form, so these equations are solved numerically using the spectral relaxation method (SRM) for Cu-water and Al_2O_3-water nanofluids with water as the base fluid (i.e. with a constant Prandtl number $Pr = 6.7850$). The thermophysical properties of the nanofluids used in the numerical simulations are given in Table 1. Extensive calculations have been performed to obtain the velocity, temperature, concentration profiles as well as skin friction, local Nusselt number and local Sherwood number for various values of physical parameters such as ϕ, M, K_1, R, Pr, Sc, δ, E_c, γ and Sr. To determine the accuracy of our numerical results, the skin friction and the heat transfer coefficient are compared with the published results of Hamad [17], Kameswaran et al. [18] and Grubka and Bobba [19]in Tables 2 and 3. Here we have varied the M with ϕ while keeping other physical parameters fixed for Cu-water and Al_2O_3-water in Table 2. It is observed that increasing the values of M results in an increase in the skin friction coefficient. The calculated values show good agreements with Hamad [17] and Kameswaran et al. [18].

In Table 3 gives a comparison of the values of wall temperature gradient $-\theta'(0)$ results with those obtained by Kameswaran et al. [18] and Grubka and Bobba [19] when $M = E_c = K_1 = \delta = R = \phi = 0$, $Sc = 1$, $Sr = 0.2$ and $\gamma = 0.08$ for different values of Prandtl number Pr. As it is shown in the table thewall temperature gradient $-\theta'(0)$ increases with an increase of Prandtl number. This is fact because the definition of Prandtl number is the ratio of kinematic viscosity to thermal diffusivity. An increase in the values of Prandtl number implies that momentum diffusivity dominates thermal diffusivity. Hence, the rate of heat transfer at the surface increases with increasing values of Pr. It is observed that the present results are in good agreement with results in the literature by Kameswaran et al. [18] and Grubka and Bobba [19]. In Table 4 approximate solutions of the skin friction coefficient, surface heat transfer and the surface mass transfer rates at different values of flow parameters are presented. All SRM results were generated using $L = 30$, $Nx = 60$ and $Nt = 1000$, these values were found to give accurate solutions after a numerical experimentation. The L and Nt in the tables represent the maximum Lth and Ntth iteration required to produce converging results. It is observed that increasing the values of Sr increase Sherwood numbers in case of Cu-water but the opposite trend is observed with Al_2O_3-water. Also increasing the values of Sc increase the Sherwood numbers for both cases of nanofluids while increasing in heat generation parameter δ is tend to decrease the heat transfer rate for both nanofluids. The table also shows that surface mass transfer rates increase with increasing in the values of the chemical reaction parameter γ as can be seen from the table.

The effects of physical parameters on various fluid dynamic quantities are show in Figures 1 - 13. Figures 1 - 4 illustrate the effect of the nanoparticle volume fraction ϕ on the velocity, temperature and concentration profiles, respectively, in the case of a Cu-water nanofluid and Al_2O_3-water nanofluid. It is clear that as the nanoparticle volume fraction increases, the Cu-water nanofluid velocity decreases while the Al_2O_3-water nanofluid velocity increases. As it is shown in Figure 1 while the temperature profile increases with increase in the values of nanoparticle volume fraction this is clear from Figure 2. increasing the volume fraction of nanoparticles increases the thermal conductivity of nanofluid and in turn results a thickening of the thermal boundary layer. It is also observed that the temperature distribution in a Cu-water nanofluid is higher than that of Al_2O_3-water nanofluid; this is an anticipated results because Cu-water is good conductor of heat and electricity. The Al_2O_3-water nanofluid concentration profile decreases as the nanoparticle volume fraction increases but reveres it true to that of Cu-water nanofluid as shown in Figure 3.

Figure 4 shows the effect of the porous medium parameter K_1 on the velocity in case of a cu-water and Al_2O_3-water nanofluids. increasing the porous medium parameter K_1 decreases the velocity profiles of both nanofluids. We observed from the Figure, the velocity profile of Al_2O_3-water nanofluid is higher than that of Cu-water nanofluid. Figures 5 and 6 show the effect of porous medium parameter K_1 on the temperature and solutal concentration profiles respectively, in the case of Cu-water and Al_2O_3-water nanofluids. It is clear that as the porous medium parameter K_1 increases the temperature and solutal concentration profiles increase.It is observed that the temperature and concentration profiles increment of Al_2O_3-water nanofluid is less than that of Cu-water nanofluid. Figure 7 illustrates the influence of heat generation parameter δ on the temperature profile in the case of Cu-water and Al_2O_3-water nanofluids. We observed that the temperature profile increases for both cases of nanofluids with increasing in the values of heat generation parameter δ. It found that the temperature in case of Cu-water is more than that of Al_2O_3-water nanofluids. Increasing the values of heat generation parameter δ increases the thermal conductivity of nanofluid and the thickening of the thermal boundary layer. Figure 8 shows the influence of the magnetic parameter M on nanofluid velocity profile in the case of Cu-water and Al_2O_3-water nanofluids. When the magnetic parameter M increases, the nanofluid velocity profile of Cu-water and Al_2O_3-water decrease. This is because of the application of the transverse magnetic field in an electrically conducting fluid produces a ratarding lorenz force slows down the fluid motion in the boundary layer and hence decreases the velocity at the expense of increasing it is temperature and the solutal concentration. But we observed the opposite for solutal concentration of Al_2O_3-water nanofluid is against this fact as illustrates in Figure 4. The velocity profile of the Al_2O_3-water nanofluid is higher than that of the Cu-water nanofluid as it shown in the Figure.

Figure 9 shows the effect of the viscous dissipation parameter E_c on the temperature profile in the case of Cu-water and Al_2O_3-water nanofluids. It is observed that the temperature profile increases of both nanofluids with increasing in the values of E_c; we notice that the influence of an increment in E_c is to increase the temperature distribution. This is due to the fact that the energy is stored in the fluid region as a consequence of dissipation because the viscosity and elastic deformation. It is observed that the temperature profile in the case of Cu-water nanofluid is higher than that of Al_2O_3-water nanofluid. Figure 10 shows the effect of the thermal radiation parameter R on the temperature profile in the case of both nanofluids. Increasing the thermal radiation Parameter R increases the temperature profile of Cu-water and Al_2O_3-water nanofluids. We observed that the temperature increases of Cu-water is higher than that of Al_2O_3-water nanofluids. The thermal radiation parameter R is responsible to thickening of thermal boundary layer. This enables the nanofluids to release the heat energy from the flow region and cases the system to be cool. This is true because of increasing the Rosseland approximation results in an increase in the temperature profile. Figure 11 illustrates the effect of the Schmidt number Sc on the solutal concentration profile in the case of Cu-water and Al_2O_3-water nanofluids. Increasing the values of Sc decreases the solutal concentration profile of both case of nanofluids. It is observed that the concentration profile of Cu-water nanofluid increases more than that of Al_2O_3-water nanofluid. Figures 12 and 13 show the effect of two parameters namely by chemical reaction parameter γ and the Soret number Sr on the concentration profiles in the case of Cu-water and Al_2O_3-water nanofluids in Figure 12 and 13 respectively. We observed that the concentration profiles decreases with an increase in the values of the scale chemical reaction parameter γ whereas the chemical reaction parameter γ effect shows no substation changes on the nanofluid velocity and temperature profile in the two case of the nanofluids. It is clear that the solutal concentration profiles in case of Al_2O_3-water nanofluid is relatively less than that of Cu-water nanofluid in Figure 12. While the Figure 13as the Soret number Sr increases, the solutal concentration boundary layer thickness of both case of nanofluids also increase. We found that the solutal concentration profiles increment of Al_2O_3-water nanofluid exhibits less than that of Cu-water nanofluid.

Conclusions

We have investigated the heat and mass transfer in steady MHD boundary layer flow in nanofluids through a porous due to an stretching surface subjected to a magnetic field, heat generation, chemical reaction, viscous dissipation and thermal radiation effects. From the numerical simulations, some results can be drawn as follow:
[i] The velocity profile of Cu-water nanofluid decreases with increasing in the nanoparticle volume fraction whereas the velocity profile of Al_2O_3-water nanofluids increases with increasing in the nanoparticle volume fraction while the velocity profile of both nanofluids decrease with an increase in magnetic and porous medium parameters.
[ii] The temperature profile of both nanofluids increase with increasing in the values of the nanoparticle volume fraction while the concentration of Al_2O_3-water nanofluids decreases with increasing in the values of the nanoparticle volume fraction and the opposite trend is observed for the concentration of Cu-water nanofluids with increasing in the values of the nanoparticle volume fraction.
[iii] The temperature profile of both nanofluids increase with increase in the values of the Viscous dissipation, heat generation and thermal radiation parameters.
[iv] The concentration profile of both nanofluids decreases with increase in the values of chemical reaction parameter and Schmidt number while the opposite trend is observed for the increasing values of the Soret number in the both case of nanofluids.
[v] The rate of thermal boundary layer thickness of both nanofluids decreases with the presence of nanoparticle volume fraction, thermal radiation, porous media and viscous dissipation in the flow field.
[vi]In general, the Al_2O_3-water nanofluid shows thicker velocity layer at the plate than a Cu-water nanofluids; Al_2O_3-water nanofluid exhibits thicker thermal and concentration boundary layer than that of a Cu-water nanofluid.

Acknowledgment:

The authors are grateful to the University of KwaZulu-Natal, South Africa for the necessary support. Also, this work is based on the research supported by the National Research Foundation, South Africa.

References

[1] Crane, L.J. (1970) Flow past a stretching plate, *ZAMP. Angew Math. Phys.* 21, 645 – 647.
[2] Khan, W.A. and Pop, I. (2010) Boundary layer flow of a nanofluid past a stretching sheet, *International Journal of Heat and Mass Transfer* 53, 2477 – 2483.
[3] Abd El-Aziz, M. (2007) Thermal-diffusion and diffusion-thermo effects on combined heat and mass transfer by hydromagnetic three-dimensional free convection over apermeable stretching surface with radiation, *Physics Letters* 372, 3, 263 – 272.

[4] Hady, F.M., Ibrahim, F.S., Abdel-Gaied, S.M. and Mohamed Eid, R. (2012) Radiation effect on viscous flow of a nanofluid and heat transfer over a nonlinearly stretching sheet, *Nanoscale Res. Lett* 7, 229.

[5] Bachok, N., Ishak, A. and Pop, I. (2012) Unsteady boundary-layer flow and heat transfer of a nanofluid over a permeable stretching/shrinking sheet, *International Journal of Heat and Mass Transfer* 55, 2102 – 2109.

[6] Rohni, A.M., Ahmad, A.S. and Ismail, Md I. and Pop, I. (2013) Flow and heat transfer over an unsteady shrinking sheet with suction in a nanofluid using Buongiorno's model, *International Communications in Heat and Mass Transfer* 43, 75 – 80.

[7] Buongiorno, J., (2006) Convective transport in nanofluids, *ASME Journal of Heat Transfer* 128, 240 – 250.

[8] Jafar, K., Nazar, R., Ishak, A., Pop, I. (2011) MHD Flow and Heat Transfer Over stretching/ shrinking sheets with external magnetic field, viscous dissipation and Joule Effects, *Canadian Journal on Chemical Engineering* 99, 1 – 11.

[9] Murthy, P.V. and Singh, P. (1997) Effect of viscous dissipation on a non-Darcy natural convection regime, *International Journal of Heat and Mass Transfer* 40, 1251 – 1260.

[10] Motsa , S.S.(2013) A New spectral relaxation method for similarity variable nonlinear boundary layer flow systems, *Chemical Engineering Communications* 16, 23 – 57.

[11] Tiwari, R.K. and Das, M.N. (2007) Heat tranfer augmentation in a two - sided lid-driven diffrentially heated square cavity utilizing nanofluids, *International Journal of Heat and Mass Transfer* 50, 2002 – 2018.

[12] Sheikholeslami, M., Bandpy, M.G., Ganji, D.D., Soleimani, S. and Seyyedi, S.M. (2012) Natural convection of nanofluids in an enclosure between a circular and a sinusoidal cylinder in the presence of magnetic field, *International Communications in Heat and Mass Transfer* 39, 1435 – 1443.

[13] Oztop, H.F. and Abu-Nada, E. (2008) Numerical study of natural convection in partially heated rectangular enclosures filled with nanofluids, *International Journal of Heat and Fluid Flow* 29, 1326 – 1336.

[14] Brinkman , H.C.(1952) The viscosity of concentrated suspensions and solution, *Journal of Chemical Physics* 20, 571 – 581.

[15] J.C., Maxwell Garnett (1904) Colours in metal glasses and in metallic films, *Philosophical Transactions of the Royal Society of London* 203, 385 – 420.

[16] Abu-Nada , E.(2008) Application of nanofluids for heat transfer enhancement of separated flows encountered in a backward facing step, *International Journal of Heat and Fluid Flow* 29, 242 – 249.

[17] Hamad, M.A.A. (2011) Analytical solution of natural convection flow of a nanofluid over a linearly stretching sheet in the presence of magnetic field, *International Communications in Heat and Mass Transfer* 38, 487 – 492.

[18] Kameswaran, P.K., Narayana, M., Sibanda, P. and Murthy, P.V. (2012) Hydromagnetic nanofluid flow due to a stretching or shrinking sheet with viscous dissipation and chemical reaction effects, *International Journal of Heat and Mass Transfer* 55, 7587 – 7595.

[19] Grubka, L.G. and Bobba, K.M. (1985) Heat transfer characteristics of a continuous stretching surface with variable temperature, *The ASME Journal of Heat Transfer* 107, 248 – 250.

Table 1. Thermophysical properties of the water and copper and alumina nanoparticles, (see Sheikholeslami et al. [12] and Oztop and Abu-Nada [13])

Physical properties	Base fluid (Water)	Copper (Cu)	Alumina (Al_2O_3)
$C_p(J/kgK)$	4179	385	765
$\rho(Kg/m^3)$	997.1	8933	3970
$k(W/mK)$	0.613	401	40
$\alpha \times 10^7(m^2/s)$	1.47	1163.1	131.7
$\beta \times 10^5(K^{-1})$	21	1.67	0.85

Table 2. Comparison of $-f''(0)$ for various values of M and ϕ when $Pr = 6.2,\ Sc = 1,\ Sr = 0.2,\ E_c = 0,\ K_1 = 0.0,\ R = 0,\ \delta = 0.02,\ \gamma = 0.08$

		Hamad[17]		Kameswaran et al.[18]		Present results	
M	ϕ	Cu-water	Al_2O_3	Cu-water	Al_2O_3	Cu-water	Al_2O_3
0	0.05	1.10892	1.00538	1.108919904	——	1.108920	1.005385
	0.1	1.17475	0.99877	1.174746021	——	1.174746	0.998781
	0.15	1.20886	0.98185	1.208862320	——	1.208862	0.981854
	0.2	1.21804	0.95592	1.218043809	——	1.218043	0.955931
0.5	0.05	1.29210	1.20441	1.292101949	——	1.292102	1.204412
	0.1	1.32825	1.17548	1.328248829	——	1.328249	1.175484
	0.15	1.33955	1.13889	1.339553714	——	1.339554	1.138892
	0.2	1.33036	1.09544	1.330356126	——	1.330356	1.095444
1	0.05	1.45236	1.37493	1.452360679	——	1.452361	1.374930
	0.1	1.46576	1.32890	1.465763175	——	1.465763	1.328901
	0.15	1.45858	1.27677	1.458581570	——	1.458582	1.276766
	0.2	1.43390	1.21910	1.433898227	——	1.433898	1.219104
2	0.05	1.72887	1.66436	1.728872387	——	1.728872	1.664356
	0.1	1.70789	1.59198	1.707892022	——	1.707892	1.591984
	0.15	1.67140	1.51534	1.671398302	——	1.671398	1.515336
	0.2	1.62126	1.43480	1.621264175	——	1.621264	1.434799

Table 3. Comparison of the values of wall temperature gradient $-\theta'(0)$ from currents with Kameswaran et al. [18] and Grubka and Bobba [19] for different values of Prandtl numbers Pr when $M = E_c = K_1 = \delta = R = 0$, $Sc = 1,\ Sr = 0.2,\ \gamma = 0.08$ and $\phi = 0$.

Pr	0.72	1	3	10	100
Kameswaran et al. [18]	1.08852	1.33333	2.50973	4.79687	15.71163
Grubka and Bobba [19]	1.0885	1.3333	2.5097	4.7969	15.7120
Present result (SRM)	1.088524	1.333333	2.509725	4.796873	15.711967

Table 4. Comparison of the SRM solutions for $f''(0)$, $-\theta'(0)$, and $-\varphi'(0)$ for different values of $Sr,\ Sc,\ \delta$ and γ. $\phi = 0.1, E_c = 1,\ M = 0.5,\ Sc = 1,\ \delta = 0.01,\ Pr = 6.2,\ K_1 = 1,\ \gamma = 0.08,\ Sr = 0.2.$

	$Cu - water$					$Al_2O_3 - water$
	$\phi = 0.1, E_c = 1$		$R = 2, Pr = 6.2$		$K_1 = 1, M = 0.5$	
Sr	$f''(0)$	$-\theta'(0)$	$-\varphi'(0)$	$f''(0)$	$-\theta'(0)$	$-\varphi'(0)$
0.0	1.662602	0.262150	1.202677	1.543296	0.387825	1.231631
0.1	1.662602	0.262150	1.203733	1.543296	0.387825	1.223237
0.3	1.662602	0.262150	1.205845	1.543296	0.387825	1.206449
0.4	1.662602	0.262150	1.206901	1.543296	0.387825	1.198055
Sc						
0.6	1.662602	0.262150	1.204789	1.543296	0.387825	1.214843
0.7	1.662602	0.262150	1.574980	1.543296	0.387825	1.587530
0.8	1.662602	0.262150	1.887968	1.543296	0.387825	1.901663
0.9	1.662602	0.262150	2.163376	1.543296	0.387825	2.177705
δ						
0.6	1.662602	2.350214	0.854174	1.543296	2.408433	0.877492
0.7	1.662602	2.305154	0.861916	1.543296	2.365163	0.884957
0.8	1.662602	2.258469	0.869887	1.543296	2.320555	0.892611
0.9	1.662602	2.044322	0.905376	1.543296	2.122996	0.925819
γ						
0.6	1.662602	0.262150	1.140069	1.543296	0.387825	1.155418
0.7	1.662602	0.262150	1.219003	1.543296	0.387825	1.228159
0.8	1.662602	0.262150	1.438686	1.543296	0.387825	1.439333
0.9	1.662602	0.262150	1.642761	1.543296	0.387825	1.639504

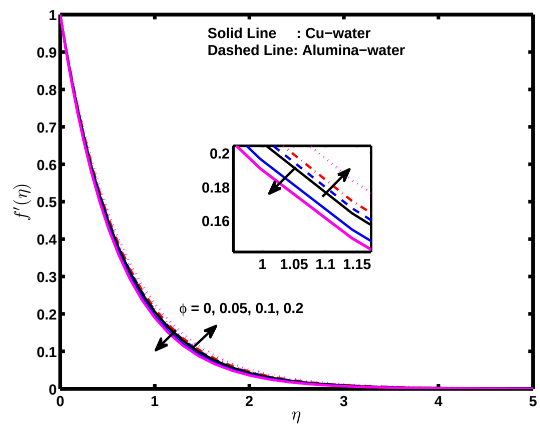

Figure 1. Effect of various nanoparticle values fraction ϕ on velocity profile for $K_1 = 1.0$, $M = 0.5$, $E_c = 1.0$, $R = 2.0$, $Pr = 6.2$, $\delta = 0.01$, $\gamma = 0.08$, $Sc = 1$ **and** $Sr = 0.4$.

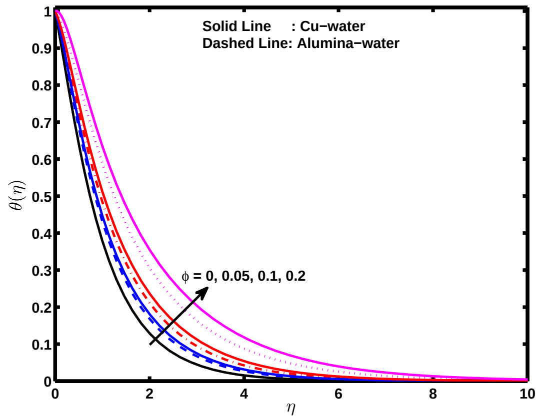

Figure 2. Effect of various nanoparticle values fraction ϕ on temperature profile for $K_1 = 1.0$, $M = 0.5$, $E_c = 1.0$, $R = 2.0$, $Pr = 6.2$, $\delta = 0.01$, $\gamma = 0.08$, $Sc = 1$ and $Sr = 0.4$.

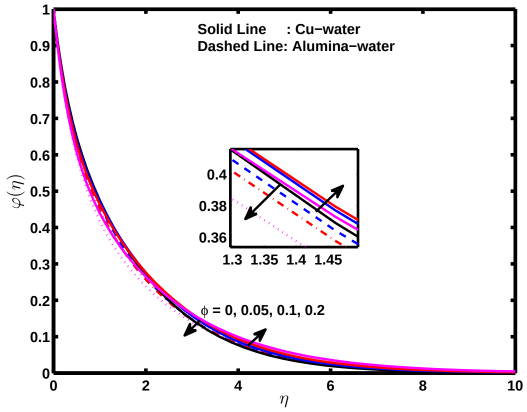

Figure 3. Effect of various nanoparticle values fraction ϕ on the concentration profile for $K_1 = 1.0$, $M = 0.5$, $E_c = 1.0$, $R = 2.0$, $Pr = 6.2$, $\delta = 0.01$, $\gamma = 0.08$, $Sc = 1$ and $Sr = 0.4$.

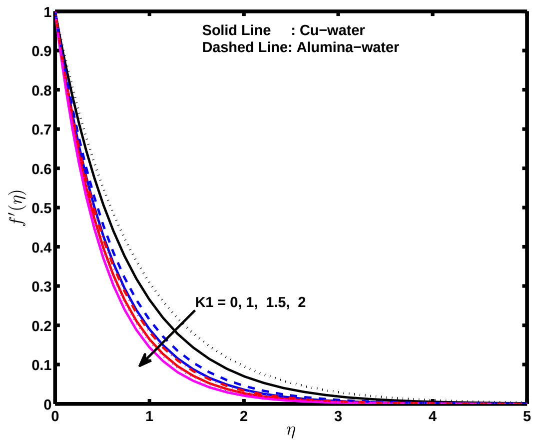

Figure 4. Effect of various nanoparticle values fraction ϕ on the velocity profile for $\phi = 0.2$, $M = 0.5$, $E_c = 1.0$, $R = 2.0$, $Pr = 6.2$, $\delta = 0.01$, $\gamma = 0.08$, $Sc = 1$ and $Sr = 0.2$.

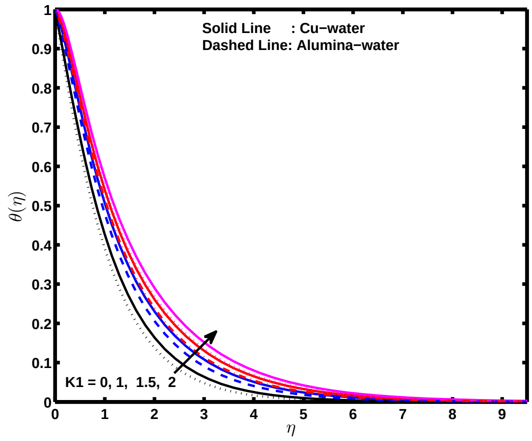

Figure 5. Effect of the porous medium parameter K_1 on temperature profile for ϕ = 0.2, M = 0.5, E_c = 1.0 , R = 2.0, Pr = 6.2, δ = 0.01, γ = 0.08, Sc = 1 and Sr = 0.2.

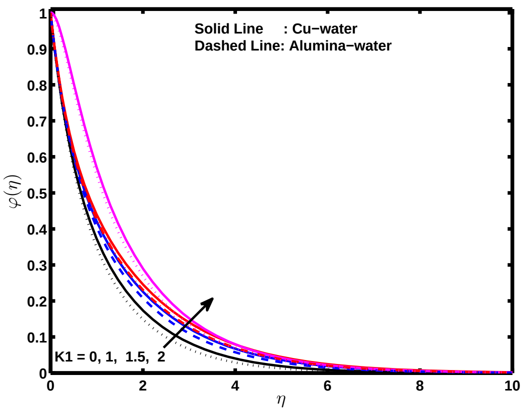

Figure 6. Effect of the porous medium parameter K_1 on concentration profile for ϕ = 0.2, M = 0.5, E_c = 1.0 , R = 2.0, Pr = 6.2, δ = 0.01, γ = 0.08, Sc = 1 and Sr = 0.2.

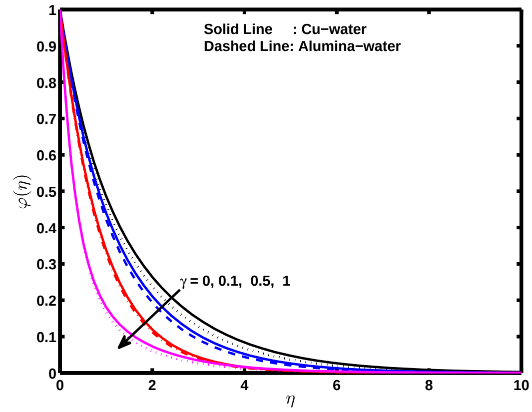

Figure 7. Effect of heat generation parameter δ on the temperature profile for $\phi = 0.2$, $M = 0.5$, $E_c = 1.0$, $R = 2.0$, $Pr = 6.2$, $K_1 = 1.0$, $\gamma = 0.08$, $Sc = 1$ and $Sr = 0.2$.

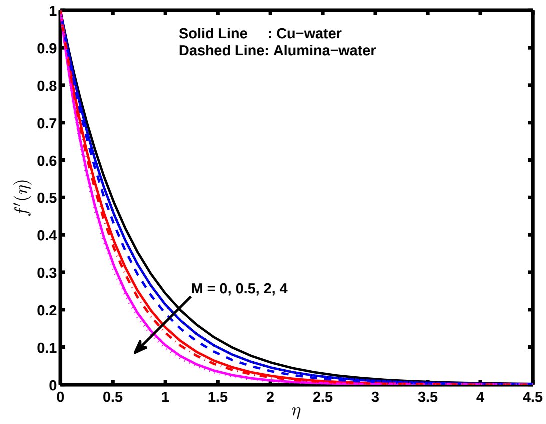

Figure 8. Effect of magnetic parameter M on the velocity profile for $\phi = 0.1$, $K_1 = 1.0$, $E_c = 1.0$, $R = 2.0$, $Pr = 6.2$, $\delta = 0.01$, $\gamma = 0.08$, $Sc = 1$ and $Sr = 0.2$.

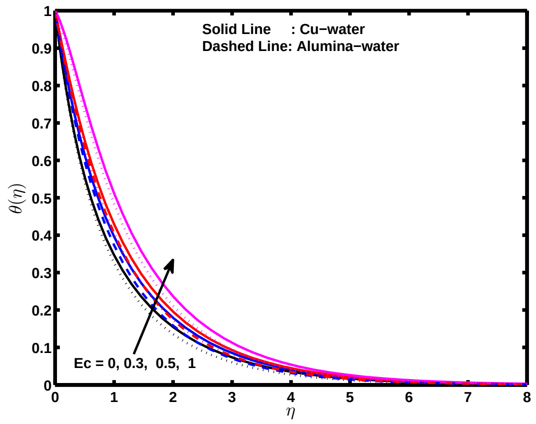

Figure 9. Effect of viscous dissipation parameter E_c on the temperature profile for $\phi = 0.1$, $K_1 = 1.0$, $M = 0.5$, $R = 2.0$, $Pr = 6.2$, $\delta = 0.01$, $\gamma = 0.08$, $Sc = 1$ and $Sr = 0.2$.

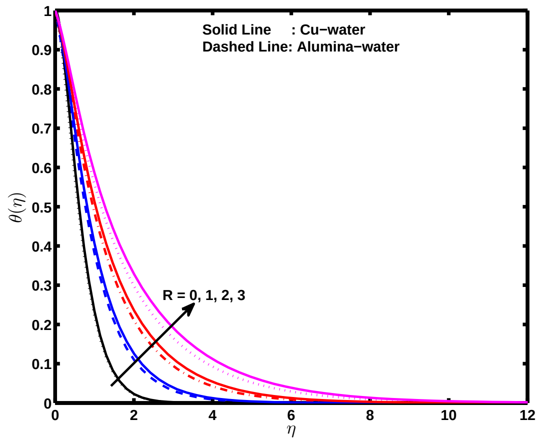

Figure 10. Effect of thermal radiation parameter R on the temperature profile for $\phi = 0.1$, $K_1 = 1.0$, $M = 0.5$, $E_c = 1.0$, $Pr = 6.2$, $\delta = 0.01$, $\gamma = 0.08$, $Sc = 1$ and $Sr = 0.2$.

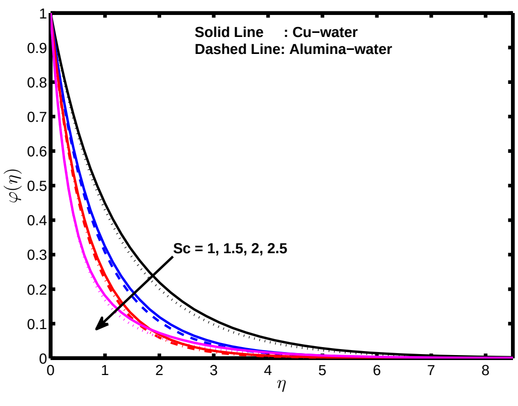

Figure 11. Effect of the Schmidt number Sc on concentration profile for $\phi = 0.1$, $K_1 = 1.0$, $M = 0.5$, $E_c = 1.0$, $Pr = 6.2$, $\delta = 0.01$, $\gamma = 0.08$, $R = 2$ and $Sr = 0.2$.

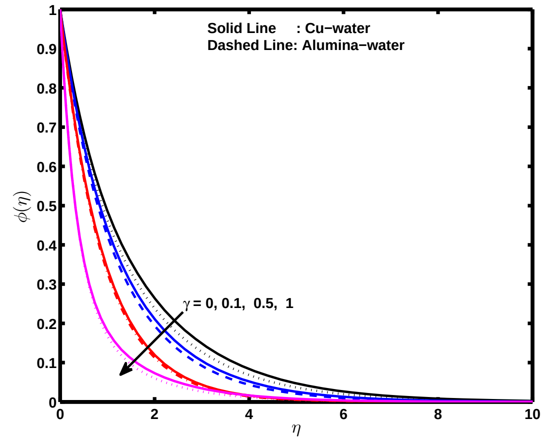

Figure 12. Effect of the chemical reaction parameter γ and Soret number Sr on concentration profiles for $\phi = 0.1$, $K_1 = 1.0$, $M = 0.5$, $E_c = 1.0$, $Pr = 6.2$, $\delta = 0.01$, $Sc = 1$ and $R = 2$.

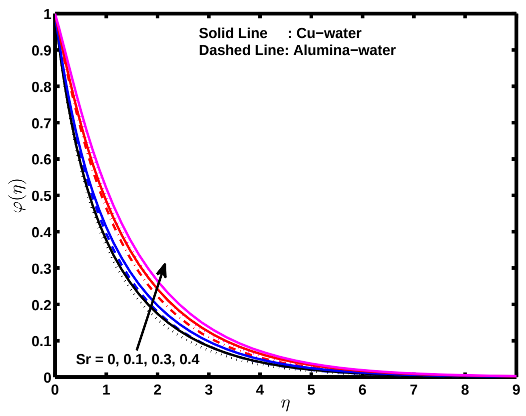

Figure 13. Effect of the chemical reaction parameter γ and Soret number Sr on concentration profiles for $\phi = 0.1$, $K_1 = 1.0$, $M = 0.5$, $E_c = 1.0$, $Pr = 6.2$, $\delta = 0.01$, $Sc = 1$ and $R = 2$.